Binuclear heterometallic {M—Ln} pivalate complexes (M = Co, Ni, Cu; Ln = Sm, Gd): synthesis, structure, and thermolysis*

E. V. Orlova,[a] A. E. Goldberg,[a] M. A. Kiskin,[a] P. S. Koroteev,[a] A. L. Emelina,[b] M. A. Bykov,[b] G. G. Aleksandrov,[a] Zh. V. Dobrokhotova,[a] V. M. Novotortsev,[a] and I. L. Eremenko[a]*

[a]*N. S. Kurnakov Institute of General and Inorganic Chemistry, Russian Academy of Sciences, 31 Leninsky prosp., 119991 Moscow, Russian Federation. Fax: +7 (495) 955 4835. E-mail: mkiskin@igic.ras.ru*
[b]*Department of Chemistry, M. V. Lomonosov Moscow State University, 1 Leninskie Gory, 119992 Moscow, Russian Federation*

Binuclear heterometallic complexes (η^2-bpy)CoLn(Piv)$_5$(H_2O), (η^2-bpy)NiLn(Piv)$_5$(H_2O), and (η^2-bpy)CuLn(Piv)$_5$(HPiv) (Ln = Sm or Gd, Piv^- is the pivalate anion) were synthesized. A comparative study of the structural characteristics and the thermolysis of the resulting compounds was performed.

Key words: heterometallic complexes, cobalt complexes, nickel complexes, lanthanide complexes, X-ray diffraction study, thermolysis.

Solid-state materials provide the basis for modern electronic technique. Ceramics were the first materials used for manufacturing electrotechnical products. Among oxide ceramic materials, complex oxides (ferrites, cobaltates, cuprates, niobates, molybdates, manganates, and other compounds of alkali, alkaline earth, and rare earth elements and their more complex combinations) are of most importance. Functional materials based on mixed rare earth, iron, manganese, cobalt. and copper oxides are used as adhesive protective coatings, optical processors, waveguides, luminophores, catalysts, and acousto-optical, data storage, and reading devices. Methods for the production of compacted complex oxides can be divided into conventional techniques for the preparation of ceramic materials and techniques involving precursors. Good characteristics as regards the improvement of functional properties of these materials can be achieved with the use of high-purity starting compounds and synthesis methods providing high chemical and phase homogeneity of the products. Compared to high-temperature solid-state synthesis, the so-called soft chemistry techniques are more promising. Of chemical methods for the synthesis of oxide materials, methods for the synthesis of oxides from vapors or solutions of organometallic compounds hold promise. Currently, powders of complex oxides are synthesized with the use of precursors in the form of solid solutions and mechanical mixtures of various compounds (salts of inorganic acids, hydroxides, complexes with organic ligands, *etc*.). However, the employment of such compounds has some drawbacks and not always results in the production of high-quality materials. Hence, it is more advantageous to prepare complex oxide materials not from mixtures but from individual heterometallic compounds. The synthesis of complex oxide systems based on heterometallic coordination compounds is performed with the use of molecular precursors, from which an organic part of the molecule is removed under relatively mild conditions (at temperatures below 400—500 °C) to form the required oxides. The composition of the target oxide and even its properties can be programmed by choosing the composition of the precursor. Studies of heterometallic complexes were started in 1960s. These compounds have attracted interest because they would be expected to have unusual properties due to the close proximity of atoms of different metals. In addition, these complexes can be used as precursors for mixed oxides, which are functional materials. Carboxylates account for the major part of these complexes. Derivatives of chelating amino acids were the first structurally characterized heterometallic 3d-3d and 3d-4f carboxylates; more recently, structures containing bridging carboxy or hydroxy ligands have been described.[1] Many 3d-4f complexes were prepared during the search for precursors of high-temperature (high-Tc) superconductors (HTS).[2—5] The synthesis of dysprosium manganese perovskites from heterometallic coordination compounds with malic and gluconic acids was described.[6] It was shown that films of samarium and neodymium nickelates can be prepared by combining epitaxial stabilization and special heterometallic complex precursors.[7] Examples of heterometallic

* Dedicated to Academician of the Russian Academy of Sciences O. M. Nefedov on the occasion of his 80th birthday.

Published in Russian in *Izvestiya Akademii Nauk. Seriya Khimicheskaya,* No. 11, pp. 2195—2208, November, 2011.
1066-5285/11/6011-2236

coordination compounds containing metals in different ratios, which can be used to synthesize a wide range of oxides at relatively low temperatures (300—500 °C) *via* thermal decomposition under various conditions, are relatively few.[8—12]

The aim of the present study was to find new molecular systems capable of generating complex oxides in the course of mild thermolysis. It was interesting to determine the conditions of the formation of binuclear molecules containing metals in the ratio M : Ln = 1 : 1 with the use of 2,2′-bipyridyl (bpy) as the structure-forming ligand and to investigate the thermolysis of the resulting heterometallic pivalate complexes with 3d metals (Co, Ni, or Cu) and 4*f* metals (Sm or Gd).

Results and Discussion

Earlier, it has been found[10] that the reaction of the binuclear cobalt(II) complex $Co_2(Piv)_4(2,4\text{-}Lut)_2$ (Piv is the pivalate anion and Lut is lutidine) with samarium(III) pivalate $Sm_2(Piv)_6(HPiv)_6$ afforded the trinuclear heterometallic complex $Co_2Sm(Piv)_7(2,4\text{-}Lut)_2$ (**1**). However, we failed to isolate the related complexes with nickel(II) and copper(II) atoms and a lanthanide atom under similar conditions. The difference in the formation of the complexes may be associated with the specific environment of the metal atoms in the final trinuclear complex **1**. Actually, the Co atoms in complex **1** are in a distorted tetrahedral environment, which is not always favorable for complexes with nickel and copper atoms, which, as a rule, prefer an octahedral, pseudooctahedral, or square-planar ligand environment in carboxylate-bridged molecules.[13—19] The use of bidentate N-donor apical ligands (for example, 2,2′-bipyridyl (bpy)) in the synthesis of complexes containing Ni, Co, and lanthanides would be expected to be successful.

It was found that the reaction of the binuclear cobalt complex $(\eta^2\text{-bpy})_2Co_2(Piv)_4(H_2O)$ with the samarium complex $Sm_2(Piv)_6(HPiv)_6$ affords the heterometallic molecule $(\eta^2\text{-bpy})CoLn(\mu\text{-Piv})_3(\eta^2\text{-Piv})_2(\eta^1\text{-}H_2O)$ (**2**), which, unlike complex **1**, contains only two metal atoms (Scheme 1).

Scheme 1

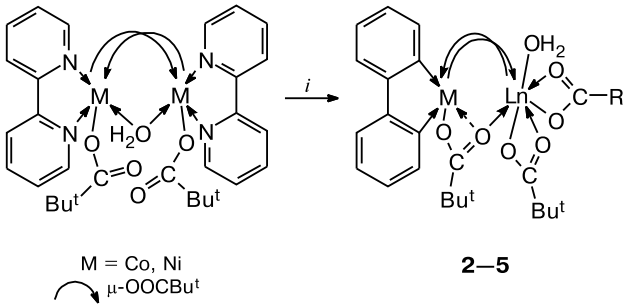

Reagents and conditions: *i*. $Ln_2(Piv)_6(HPiv)_6$ (Ln = Sm, Gd), Ln : M = 1 : 1, MeCN, 80 °C, O_2.

Atom	**2**	**3**	**4**	**5**
M	Co	Ni	Co	Ni
Ln	Sm	Sm	Gd	Gd

In complex **2**, the Sm and Co atoms are linked by three bridging pivalate groups (Co...Sm, 3.899(1) Å; Co—O,

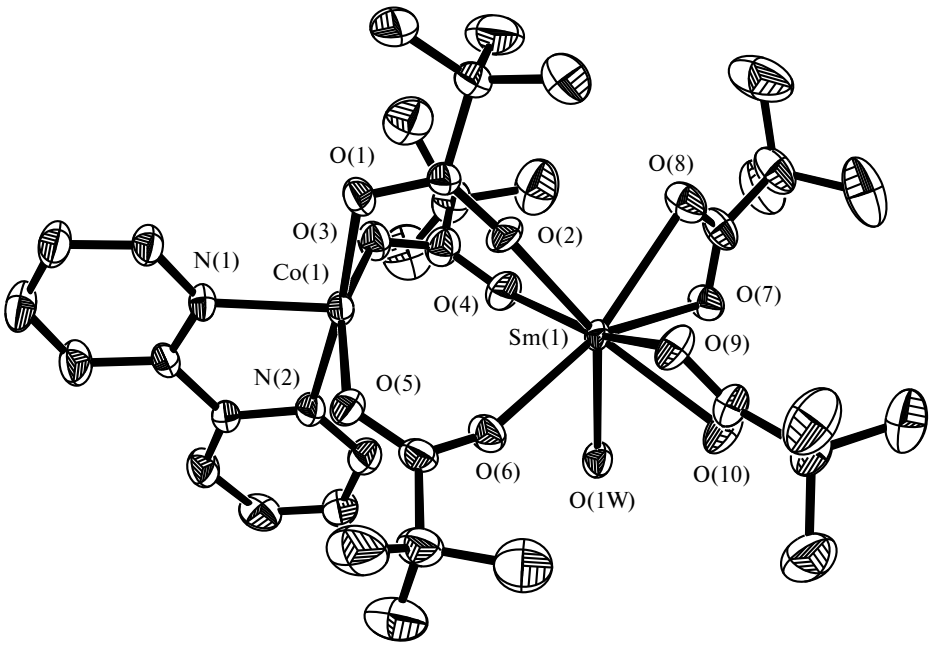

Fig. 1. Structure of complex **2** (hydrogen atoms are omitted, thermal ellipsoids are drawn at the 30% probability level).

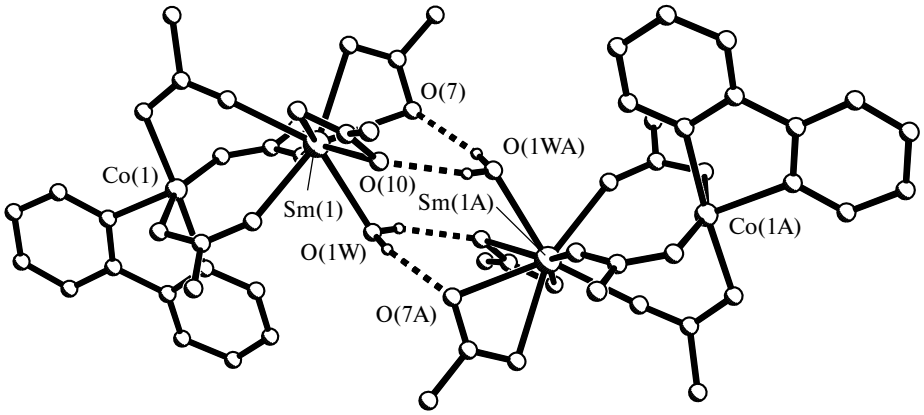

Fig. 2. Fragment of the molecular packing of complex **2** (hydrogen atoms and methyl substituents at the carboxylate groups are omitted).

2.009(5)—2.048(5) Å; Sm—O, 2.321(5)—2.350(5) Å) (Fig. 1). The environment of the Sm atom can be described as a distorted dodecahedron (a monocapped pentagonal bipyramid) formed due to the additional coordination of Sm to two chelating carboxylate groups and one water molecule (Sm—O(Piv), 2.418(5)—2.544(5) Å; Sm—O(H_2O), 2.471(5) Å). The coordination polyhedron of the Co atom is completed to a distorted tetragonal pyramid ($\tau = 0.25$)[20] through the coordination to two N atoms of the bpy molecule (Co—N, 2.088(6) and 2.171(6) Å). In the crystal, the neighboring complexes are symmetrically linked by hydrogen bonds between water molecules and carboxylate groups (O(1W)—H, 0.83 Å; O(1W)...O(7)*, 2.92 Å; H...O(7)*, 2.14 Å; O(1W)—H—O(7)*, 159.1°; O(1W)—H, 0.83 Å; O(1W)...O(10)*, 2.74 Å; H...O(10)*, 2.01 Å; O(1W)—H—O(10)*, 146.4°) (Fig. 2).

*1 – x, –y, –z.

Under the conditions analogous to those resulting in the formation of compound **2**, the reaction of $Sm_2(Piv)_6(HPiv)_6$ with $(\eta^2\text{-bpy})_2Ni_2(Piv)_4(H_2O)$ affords the binuclear complex $(\eta^2\text{-bpy})NiSm(\mu\text{-Piv})_2(\mu,\eta^2\text{-Piv})(\eta^2\text{-Piv})_2(\eta^1\text{-}H_2O)$ (**3**) (see Scheme 1), which crystallizes as a solvate with two pivalic acid molecules (**3**·2HPiv). In complex **3**, the Sm and Ni atoms are linked by two bridging and one chelating bridging pivalate groups (Ni...Sm, 3.7533(6) Å; Ni—O, 2.0158(18)—2.3417(19) Å; Sm—O, 2.3262(19)—2.3831(18) Å). The Sm atom coordinates two chelating carboxylate groups and one water molecule (Sm—O(Piv), 2.445(2)—2.501(2) Å; Sm—O(H_2O), 2.433(2) Å); the Ni atom coordinates the bpy molecule (Co—N, 2.035(2) and 2.062(2) Å) (Fig. 3). As a result, as opposed to compound **2**, the transition metal in molecule **3** is in an octahedral rather than tetragonal ligand environment.

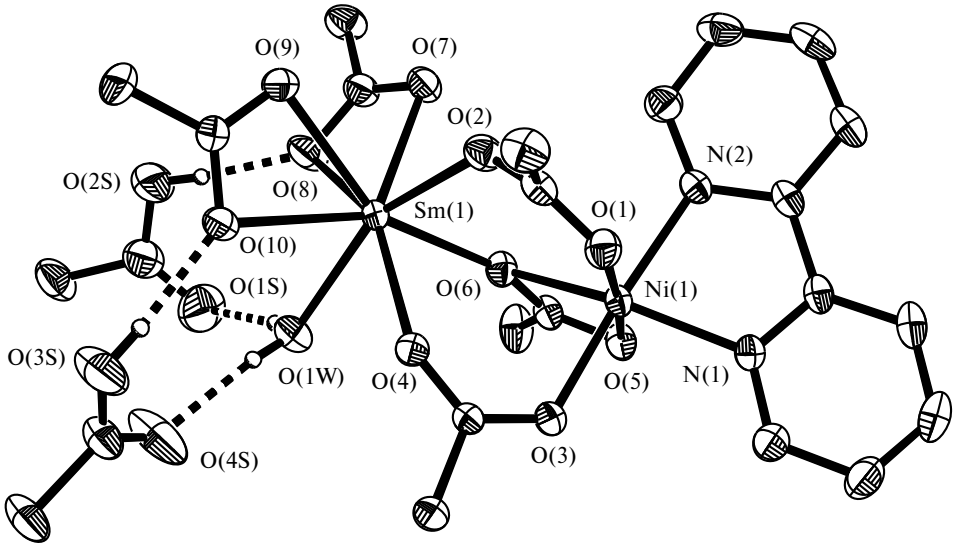

Fig. 3. Structure of complex **3**·2HPiv (hydrogen atoms and methyl substituents at the carboxylate groups are omitted, thermal ellipsoids are drawn at the 30% probability level).

There are hydrogen bonds between the H atoms of the coordinated water molecule and two O atoms of two HPiv solvent molecules (O(1W)—H 0.82 Å, O(1W)...O(1S), 2.78 Å; H...O(1S), 1.99 Å; O(1W)—H—O(1S), 163.5°; O(1W)—H, 0.83 Å; O(1W)...O(4S), 2.71 Å; H...O(4S), 1.90 Å; O(1W)—H—O(4S), 170.6°). The H atoms of the acid solvent molecules are, in turn, involved in hydrogen bonding with the oxygen atoms of the chelating carboxylate groups (O(2S)—H, 0.82 Å; O(2S)...O(8), 2.64 Å; H...O(8), 1.82 Å; O(2S)—H—O(8), 174.2°; O(3S)—H, 0.82 Å; O(3S)...O(10), 2.66 Å; H...O(10), 1.85 Å; O(3S)—H—O(10), 170.3°). Therefore, the hydrogen bonding of binuclear molecules observed for complex **2**, is impossible in the case of complex **3** because the water molecule is blocked by acid solvent molecules. In the crystal structure, there are stacking interactions between the pyridyl rings of adjacent molecules (the shortest C(29)...C(31)* distance is 3.324(4) Å) (Fig. 4).

The replacement of one lanthanide by another one has no effect on the composition of the final product. The complexes (η^2-bpy)CoGd(Piv)$_5$(H_2O) (**4**) and (η^2-bpy)-NiGd(Piv)$_5$(H_2O)·2HPiv (**5**·2HPiv) were isolated according to similar procedures, but gadolinium nitrate was used instead of samarium nitrate. The identity of the composition of the isolated compounds was confirmed by elemental analysis (C, H, N) and the comparison of their IR spectra (see the Experimental section).

The heterometallic {Cu—Ln} complexes were synthesized with the use of $Cu_2(Piv)_4(HPiv)_2$, bpy, and $Ln_2(Piv)_6(HPiv)_6$ (Ln = Sm, Gd). As a result, crystals of the binuclear complexes (η^2-bpy)CuLn(μ-Piv)$_2$(μ,η^2-Piv)-(η^2-Piv)(η^1-Piv)(η^1-HPiv) (Ln = Sm (**6**), Gd (**7**)) were isolated in the course of the reaction.

Compound **7** is the molecular binuclear heterometallic complex. As in complexes **2** and **3**, the metal atoms in **7** (Cu(1)...Gd(1), 3.819(2) Å) are linked by two bridging and one chelating bridging carboxylate groups. The Cu atom is in a distorted trigonal-bipyramidal environment (τ = 0.63)[20] formed by three O atoms of the carboxylate groups (Cu—O, 1.915(6), 1.958(6), 2.303(7) Å) and two N atoms of the bpy molecule (Cu—N, 1.972(8), 2.051(7) Å) (Fig. 5). The environment of the Gd atom is completed to a distorted dodecahedron (a square antiprism) through the coordination to four O atoms of two bridging and one chelating bridging carboxylate groups (Gd—O, 2.247(6)—2.479(7) Å), three O atoms of the chelating and monodentate anions (Gd—O, 2.303(7)—2.447(6) Å), and one O atom of the HPiv molecule (Gd—O, 2.329(6) Å). In complex **7**, the Gd atom coordinates the chelating bridging pivalate anion. This is the feature that distinguishes complex **7** from compound **2**, which contains bridging anions coordinated to the Sm atom in a monodentate fashion, and compound **3**, in which the bridging and chelating bridging anions are coordinated to the Sm atom in a monodentate fashion.

In complex **7**, there is a hydrogen bond between the H atom of the coordinated HPiv molecule and the O atom of the monodentate Piv^- anion (O(12)—H, 0.82 Å; O(12)...O(10), 2.43 Å; H...O(10), 1.64 Å; O(12)—H—O(10), 159.2°).

The identity of compound **6** with compound **7** was confirmed by comparing their IR spectra and the results of elemental analysis (see the Experimental section).

The study of the thermolysis of complexes **2** and **4** showed that the first endothermic step in the thermal transformations both under an inert atmosphere and in air (50—95 °C) occurs without weight loss (Fig. 6, *a*). Presumably, this transformation is associated with the breaking of hydrogen bonds between the H atoms of the coordinated water molecules and the O atoms of the carbonyl group of the pivalate anion (*i.e.*, the supramolecular structure is destroyed). The thermal effect (Q) in this step is 33.6±1.8 and 30.6±1.8 kJ (mol of the complex)$^{-1}$) for complexes **2** and **4**, respectively. By assuming that there are two hydrogen bonds per molecule of the complex, the hydrogen bond energy can be considered to be almost equal within experimental error for both complexes (16.8±0.9 and 15.3±0.9 kJ (mol of the complex)$^{-1}$), and these values

*1 – x, –y, –z.

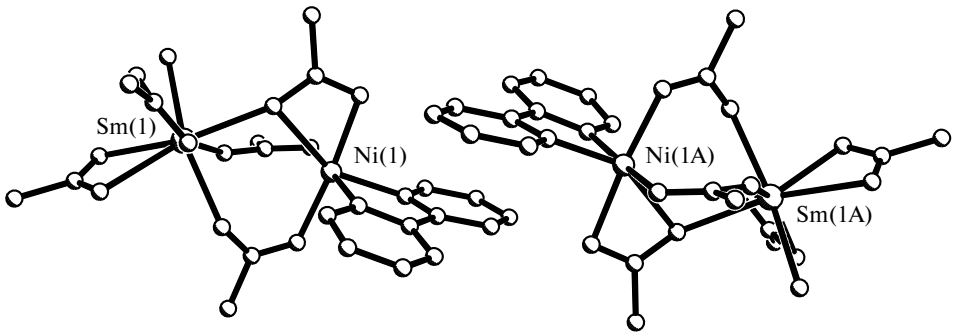

Fig. 4. Fragment of the molecular packing of complex **3** (hydrogen atoms and methyl substituents at the carboxylate groups are omitted).

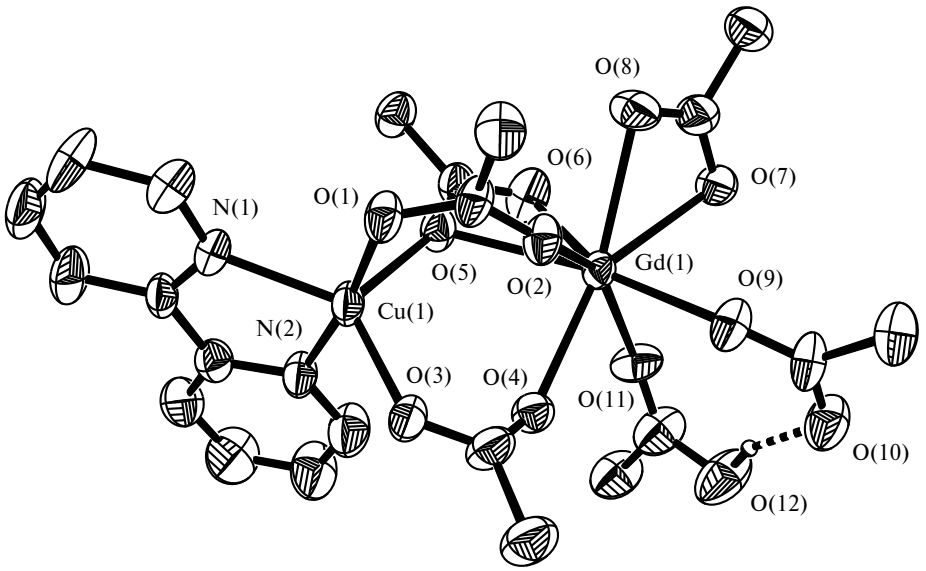

Fig. 5. Structure of complex **7** (hydrogen atoms and methyl substituents at the carboxylate groups are omitted, thermal ellipsoids are drawn at the 30% probability level).

are comparable with the hydrogen bond energy published in the literature.[21]

On heating the complex under an inert atmosphere, it undergoes decomposition in the temperature range of 100—340 °C, which is associated with the elimination of coordinated H_2O and bpy molecules (H_2O, 100—150 °C; bpy, 150—340 °C). This step is endothermic, the effect being described by a curve with complex shape (Fig. 6, *c*). In this temperature range, the weight loss is 28.3±1.5% at a heating rate of 10 deg min^{-1}, which is substantially larger than the H_2O and bpy content calculated from the empirical formula of compound **2** (19.57%). When complex **2** was heated to 250 °C under the conditions of the thermogravimetric experiment, the characteristic blue-violet deposit (trace amounts) was formed on container lids. According to the X-ray powder diffraction data, the thermolysis under an inert atmosphere at a heating rate of 10 deg min^{-1} affords a mixture of CoO and Sm_2O_3 phases (Table 1), the content of the cobalt oxide being low.

Earlier,[22,23] we have shown that the thermal decomposition of Co^{II} pivalate complexes of different nuclearity in the temperature range of 190—220 °C leads to the aggregation and the formation of the octanuclear complex $Co_8(\mu_4\text{-}O)_2(\mu_2\text{-}Piv)_6(\mu_3\text{-}Piv)_6$ (**8**). Apparently, the decomposition of complex **2** in the temperature range of 190—250 °C is accompanied by the aggregation and the formation of a similar volatile octanuclear complex. To verify this assumption and perform the experiment under nearly equilibrium conditions, the thermolysis was studied by thermogravimetry at a lower heating rate. On heating at a rate of 2 deg min^{-1} (Fig. 6, *c*) in the temperature range of 175—375 °C, the weight loss of 37.2±1.5% was recorded, which is equal within experimental error to the value calculated from the empirical formula (38.7%; the calculation was performed on the assumption that compound **8** and bpy are removed). In the temperature range of 340—510 °C, the complex undergoes further destruction accompanied by a considerable energy release, which may be associated with the formation of new structures of the solid decomposition product. According to the X-ray powder diffraction data, the thermolysis under an inert atmosphere at a heating rate of 2 deg min^{-1} produces only samarium oxide Sm_2O_3 (see Table 1).

In the investigation of the thermolysis of complex **4** under an inert atmosphere, we took into account the results obtained for complex **2**. The step associated with removal of coordinated H_2O and bpy molecules and volatile complex **8** is accompanied by a complex endothermic effect in the temperature range of 108—368 °C (Fig. 6, *a*, *b*). In this temperature range, the weight loss is 40.0±1.5%, which is equal within experimental error to the value calculated from the empirical formula (40.56%, (the calculation was performed on the assumption that H_2O, bpy, and compound **8** are removed). In the temperature range of 368—510 °C, the complex undergoes further destruction accompanied by a substantial exothermic effect, which may be associated with the formation of new structures of the solid decomposition product. The total weigh loss in the temperature range under study is 79.3±1.5%. According to the X-ray powder diffraction data, the thermolysis affords only Gd_2O_3 as the solid product (see Table 2). The thermogravimetric analysis showed that the weight of the solid product heated under an inert atmosphere accounts for 20.7±1.5% of the initial weight of the sample. This value is equal within experimental error to the value

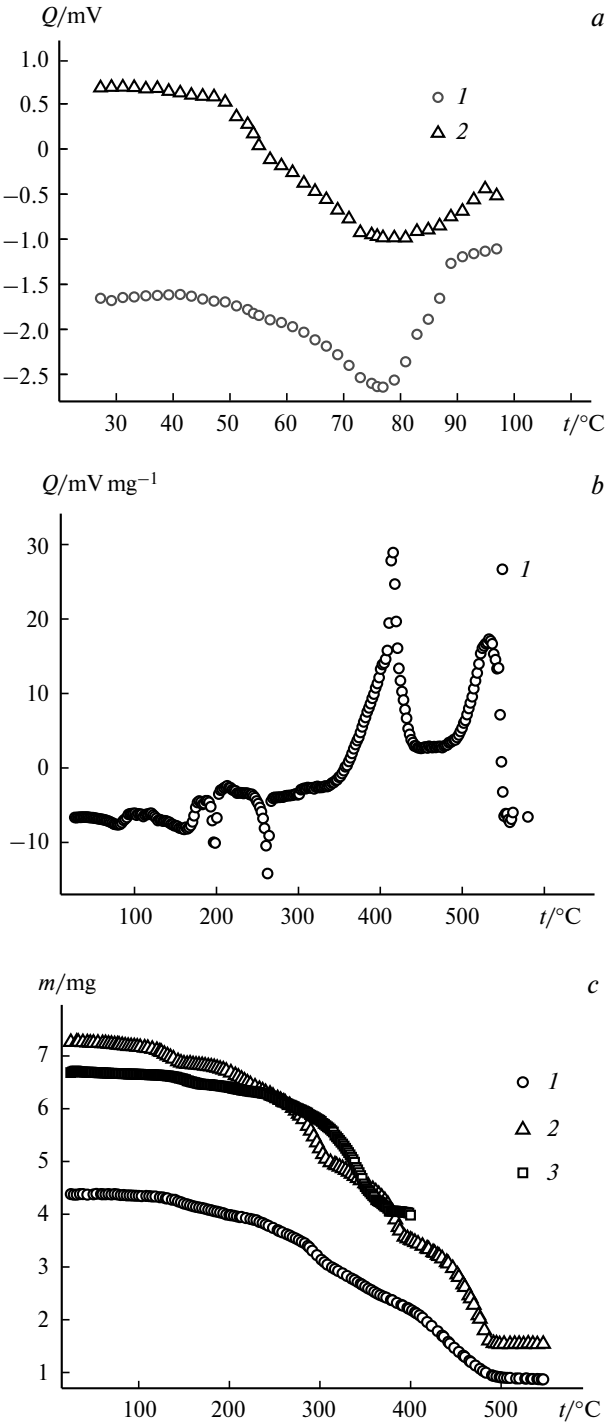

Fig. 6. DSC curves describing changes in the heat flux for complexes **2** (*1*) and **4** (*2*) during heating under an inert atmosphere in the ranges of 25—100 °C (*a*) and 25—580 °C (*b*). The weight loss for complexes **2** (*1*) and **4** (*2*) in the range of 25—580 °C at a heating rate of 10 deg min^{-1} and for complex **2** (*3*) in the range of 25—395 °C at a heating rate of 2 deg min^{-1} (*c*).

of 20.22% calculated from the empirical formula on the assumption that the thermolysis gives Gd_2O_3.

At least three steps are observed in the DSC curves obtained for compounds **2** and **4** on heating in air (Fig. 7). As in the case of heating under an inert atmosphere, the first step (below 100 °C) described by an endothermic peak, apparently, corresponds to the hydrogen bonding cleavage, and is not accompanied by weight loss. The second step exhibits an endotherm. In this step, the weigh loss (270 °C) is 20.5±1.5% and 21.0±1.5% for compounds **2** and **4**, respectively, which is equal within experimental error to the values calculated from the empirical formula (19.57 (**2**) and 19.44% (**4**); the calculations were performed on the assumption that H_2O and bpy are removed). The third step shows an exotherm and is, apparently, associated with the further destruction, the oxidation of intermediate decomposition products, and the formation of new structures. The total weigh loss in the temperature range under examination is 71.3±1.5 (**2**) and 71.5±1.5% (**4**). According to the X-ray powder diffraction data, the solid product obtained by thermolysis of compound **2** in air contains only $SmCoO_3$ (see Table 1). The thermogravimetric analysis showed that the weight of the solid product after heating in air accounts for 28.7±1.5% of the initial

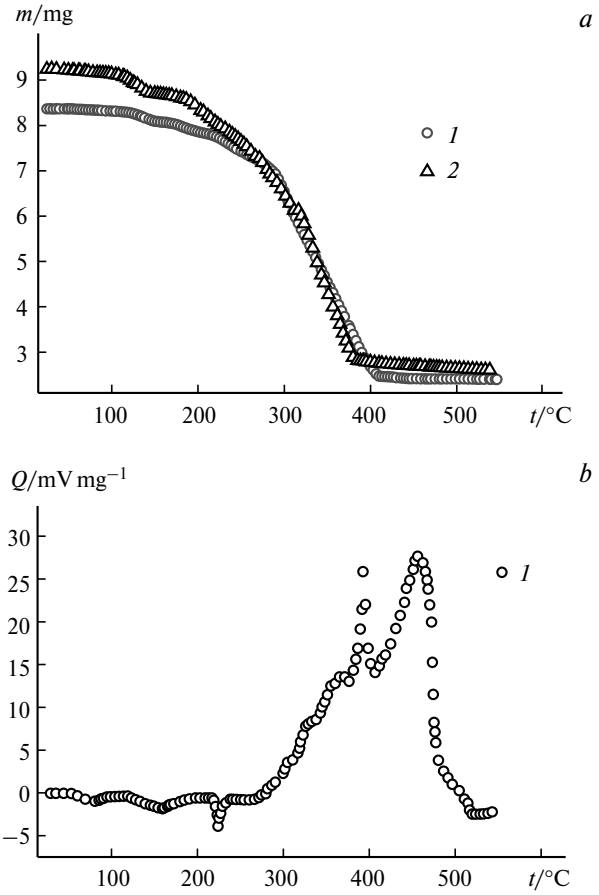

Fig. 7. Temperature dependences of the weight loss (*a*) and the heat flux (*b*) on heating complexes **1** (*1*) and **2** (*2*) in air according to the DSC data.

Table 1. X-ray powder diffraction study of the solid decomposition product of **2**

Decomposition product						$SmCoO_3$ [25 – 1071][c]		CoO [48 – 1719][c]		Sm_2O_3 [42 – 1461][c]	
in air[a]		in Ar									
		v_1[a]		v_1[b]							
d/Å	*I* (%)	*d*/Å	*I* (%)	*d*/Å	*I* (%)	*d*/Å	*I* (%)	*d*/Å	*I* (%)	*d*/Å	*I* (%)
3.745	10	—	—	—	—	3.7500	16	—	—	—	—
—	—	3.165	80	3.165	80	—	—	—	—	3.156	100
—	—	2.745	50	2.745	50	—	—	—	—	2.733	47
2.680	20	—	—	—	—	2.6740	30	—	—	—	—
2.650	100	—	—	—	—	2.6480	100	—	—	—	—
—	—	2.460	10	—	—	—	—	2.4602	65	—	—
2.180	5	—	—	—	—	2.1770	10	—	—	—	—
2.160	5	—	—	—	—	2.1580	12	—	—	—	—
—	—	2.130	30	—	—	—	—	2.1307	100	—	—
—	—	1.940	20	1.940	20	—	—	—	—	1.9326	30
1.880	40	—	—	—	—	1.8770	35	—	—	—	—
1.820	5	—	—	—	—	1.8240	10	—	—	—	—
1.650	5	—	—	—	—	1.6500	10	—	—	—	—
—	—	—	—	1.650	15	—	—	—	—	1.6478	21
—	—	—	—	—	—	—	—	—	—	1.5778	4
1.540	10	—	—	—	—	1.5410	18	—	—	—	—
1.530	20	—	—	—	—	1.5280	35	—	—	—	—
—	—	1.510	10	—	—	—	—	1.5066	54	—	—

[a] The heating rate is 10 deg min^{-1}.
[b] The heating rate is 2 deg min^{-1}.
[c] *Powder Diffraction File*, Swarthmore: Joint Committee on Powder Diffraction Standards.

weight, which is equal within experimental error to the value calculated from the empirical formula (28.9%, the calculation was performed on the assumption that the decomposition affords only $SmCoO_3$). According to the X-ray powder diffraction data, the solid thermolysis product of **4** contains only Gd_2O_3 and Co_3O_4 in a ratio close to 3 : 2 (Table 2).

Table 2. X-ray powder diffraction study of the solid decomposition product of **4**

Decomposition product				Co_3O_4 [43 – 1003][c]		Gd_2O_3 [24 – 0430][c]	
in air[a]		in Ar[b]					
d/Å	*I* (%)	*d*/Å	*I* (%)	*d*/Å	*I* (%)	*d*/Å	*I* (%)
3.350	30	3.350	20	—	—	3.345	40
3.100	10	3.090	20	—	—	3.082	20
2.950	80	2.940	100	—	—	2.940	100
2.850	20	—	—	2.8580	33	—	—
2.440	100	—	—	2.4374	100	—	—
2.320	5	—	—	2.3337	9	—	—
2.265	10	2.260	20			2.265	20
2.040	10	—	—	2.0210	20	—	—
1.930	5	1.935	10	—	—	1.932	15
—	—	—	—	—	—	1.751	10
1.645	15	—	—	1.6501	9	—	—
—	—	1.635	20	—	—	1.637	15
—	—	—	—	—	—	1.617	10
1.555	20	—	—	1.5558	32	—	—

[a] The heating rate is 10 deg min^{-1}.
[b] The heating rate is 2 deg min^{-1}.
[c] *Powder Diffraction File*, Swarthmore: Joint Committee on Powder Diffraction Standards.

Complexes **3** · 2HPiv and **5** · 2HPiv, like compounds **2** and **4**, are characterized by the presence of hydrogen bonds, although the hydrogen bonds in the former two compounds are intramolecular. On heating to 95 °C both under an inert atmosphere and in air, endothermic effects (Fig. 8, *a*) without weight loss (Fig. 8, *c*) were apparently associated with the hydrogen bond cleavage. In this step, the thermal effect is 74.4±2.4 and 76.6±2.4 (Q, kJ mol^{-1} of the complex) for complexes **3** · 2HPiv and **5** · 2HPiv, respectively. The structural data are inconsistent with the assumption that all intramolecular hydrogen bonds are equivalent.

The first decomposition step of the complexes shows endotherms both under an inert atmosphere and in air (see Fig. 8, *b*). The DSC curves show a doubled endothermic peak. For complex **3**, Q = 215.2±4.9 (in Ar) and 218.0±4.9 kJ mol^{-1} (in air) in the temperature range of 96—210 °C and 96—192 °C, respectively; the weight loss is 19.5±1.5% under an inert atmosphere and 20.6±1.5% in air. For complex **5**, Q = 218.2±4.9 (in Ar) and 219.0±4.9 kJ mol^{-1} (in air) in the temperature range of 102—228 °C and 102—206 °C, respectively; the weight loss is 20.4±1.5% under an inert atmosphere and 20.1±1.5% in air. The presence of two HPiv molecules and one H_2O molecule in complexes **3** and **5** evaluated from the empirical formula is 20.31 and 20.18%, respectively (the enthalpy of the evaporation of HPiv at the boiling point is 73.2 kJ mol^{-1}, and the enthalpy of the evaporation of H_2O is 40.6 kJ mol^{-1}).[24]

Therefore, taking into account the weight loss and the the quantity of the absorbed energy, it can be assumed that the first step results in the removal of two pivalic acid solvent molecules and the coordinated water molecule. Unlike the thermolysis of cobalt-containing complexes, complexes **3** and **5** are characterized by the formation of a certain intermediate stable in a rather broad temperature range; for complex **3**, this range is 210—265 °C under argon and 190—244 °C in air; for complex **5**, 228—282 °C under argon and 206—261 °C in air). At higher temperatures, the further weight loss accompanied by complex energy changes is observed. We failed to distinguish steps in the course of the further destruction. The thermolysis of **3** is completed at 480 °C under argon and at 455 °C in air; for **5**, at 495 °C under argon and at 475 °C in air. The total weight loss in the temperature range under study is 78.0±1.5% under an inert atmosphere and 77.1±1.5% in air for **3** and, correspondingly, 78.2±1.5% and 76.5±1.5% for **5**. According to the X-ray powder diffraction data, the solid thermolysis product obtained in air contains rare earth metal oxides (Sm_2O_3 and Gd_2O_3) and NiO (Table 3). The thermogravimetric analysis showed that, after heating in air, the weight of the solid product accounts for 22.8±1.5% for **3** and 23.5±1.5% for **5** of the initial weight. These values are equal within experimental error to the values calculated from the empirical formula (22.69% (**3**) and 23.18% (**5**); the calculations were performed on the assumption that the decomposition affords a mixture of oxides $LnO_{1.5}$ and NiO). The thermolysis of compounds **3**

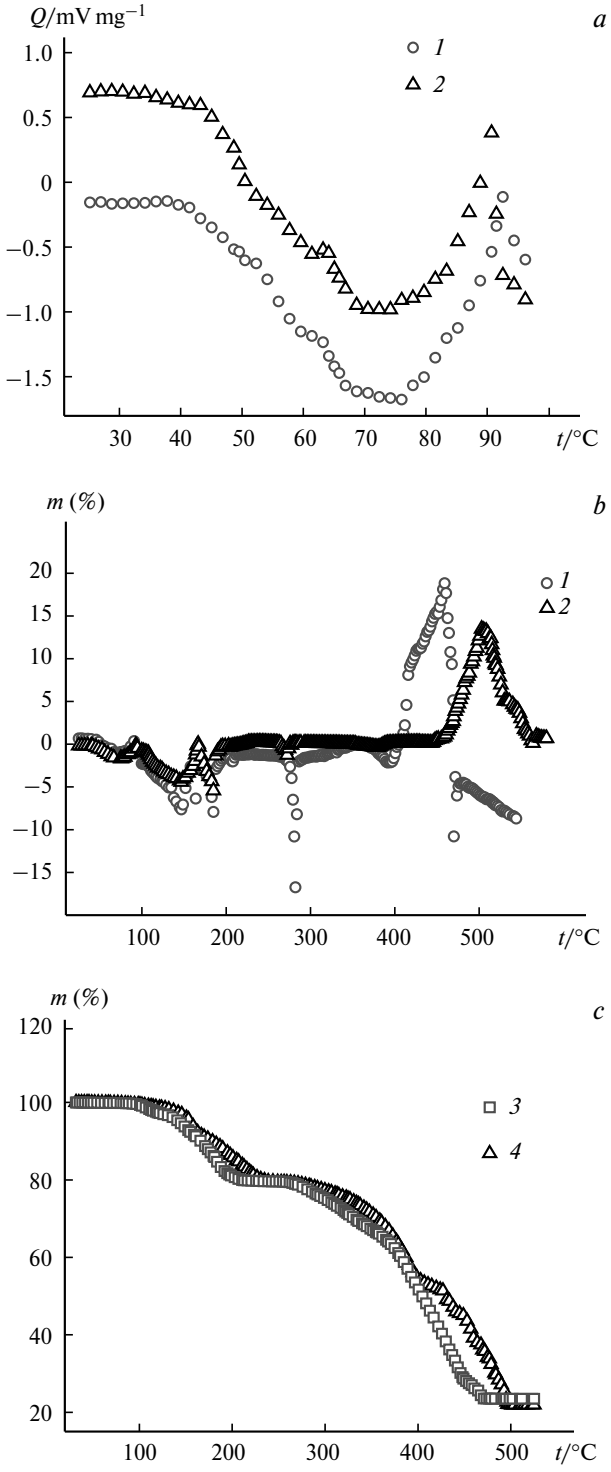

Fig. 8. DSC curves describing changes in the heat flux for compounds **3** · 2HPiv (*1*) and **5** · 2HPiv (*2*) during heating under an inert atmosphere in the ranges of 25—100 °C (*a*) and 25—580 °C (*b*). The weight loss for **5** · 2HPiv in the temperature range of 25—530 °C (*c*) in argon (*3*) and in air (*4*).

Table 3. X-ray powder diffraction study of the solid decomposition product of **3**

Decomposition product				Ni [04 – 0850]*		NiO [44 – 1159]*		Sm_2O_3 [42 – 1461]*	
in air		in Ar							
d/Å	*I* (%)	*d*/Å	*I* (%)	*d*/Å	*I* (%)	*d*/Å	*I* (%)	*d*/Å	*I* (%)
3.160	60	3.165	80	—	—	—	—	3.156	100
2.750	40	2.745	50	—	—	—	—	2.733	47
2.420	60	—	—	—	—	2.4119	60	—	—
2.080	100	—	—	—	—	2.0884	100	—	—
—	—	2.040	100	2.034	100	—	—	—	—
1.940	10	1.940	20	—	—	—	—	1.9326	30
—	—	1.760	30	1.762	42	—	—	—	—
1.650	10	1.650	10	—	—	—	—	1.6478	21
1.580	5	—	—	—	—	—	—	1.5778	4

* *Powder Diffraction File*, Swarthmore: Joint Committee on Powder Diffraction Standards.

and **5** under an inert atmosphere produces a mixture of the phases Ni and Ln_2O_3. According to the TGA data, the weight of the solid product heated under an inert atmosphere accounts for 22.0±1.5% for **3** and 21.8±1.5% for **5** of the initial weight, which is equal within experimental error to the values calculated from the molecular formula (21.22% and 21.82%, respectively, on the assumption that the decomposition gives a mixture of Ln_2O_3 and Ni).

The stepwise character of the decomposition of complexes **6** and **7** is more pronounced compared to complexes **2**—**5**. Let us consider the results of the thermolysis performed in air. The thermolysis is observed at temperatures above 100 °C (Fig. 9). The peak describing the weight loss in the first step (at temperatures below approximately 180 °C) precedes a nearly horizontal region. In the above-mentioned temperature range, the gas-phase mass spectrum shows ion peaks corresponding to the ionization of pivalic acid molecules (CO_2^+, $C_2H_3^+$, $C_2H_5^+$, $C_3H_5^+$, $C_3H_7^+$, $C_4H_9^+$).[23] However, the mass spectrum does have ion peaks corresponding to the ionization of bipyridyl ($C_{10}H_8N_2^+$, $C_{10}H_7N_2^+$, $C_{10}H_8^+$, $C_5H_4N^+$, $C_4H_3^+$),[25] although their intensities are low. The weight losses (Δm = = 10.0±1.5% (**6**) and Δm = 9.7±1.5% (**7**)) are consistent within experimental error with the calculated mass content of coordinated HPiv molecules (10.44% (**6**) and 10.34% (**7**)).

As can be seen from Fig. 9, *c*, the endothermic effects of the first and second thermolysis steps are well-resolved. Apparently, the decomposition of the complexes in the first step is mainly associated with the removal of coordinated pivalic acid. The second decomposition step in the temperature range of 180—290 °C is accompanied by an endothermic effect that precedes an exothermic peak; the weight loss is 14.8±1.5% (**6**) and 15.1±1.5% (**7**), which is consistent within experimental error with the calculated mass content of coordinated bpy molecules (15.97% (**6**) and 15.86% (**7**)). The third exothermic step reflects, apparently, the deeper destruction, the oxidation of intermediate decomposition products, and the formation of new structures. The weight loss is completed at 400 °C, whereas the processes accompanied by energy changes terminate at higher temperature. According to the TGA data, the weight of the solid product after heating in air accounts for 25.0±1.5% for **6** and 25.4±1.5% for **7** of the initial weight, which is equal within experimental error to the values calculated from the empirical formula (25.96% for **6** and 26.62% for **7**). The calculations were performed on the assumption that the decomposition product is a mixture of CuO and Ln_2CuO_4. According to the X-ray powder diffraction data, the solid thermolysis product obtained in air contains CuO and Ln_2CuO_4 (Table 4).

The non-isothermal TGA curves of complex **6** were analyzed. The formal mechanism of the process was simulated with the use of the NETZSCH Thermokinetics

Table 4. X-ray powder diffraction study of solid decomposition product of **6**

Decomposition product in air		CuO [48 – 1548]*		Sm_2CuO_4 [24 – 0998]*	
d/Å	*I* (%)	*d*/Å	*I* (%)	*d*/Å	*I* (%)
2.77	70	—	—	2.780	100
2.75(br)	20	—	—	2.760	30
		2.7520	13	—	—
2.53	20	2.5323	37	—	—
2.515	100	2.5236	100	—	—
2.31(br)	70	2.3242	99	—	—
		2.3131	21	—	—
2.03	10	—	—	2.026	20
1.99	5	—	—	1.989	10
1.95	15	—	—	1.952	25
1.67	20	1.8676	30	—	—

**Powder Diffraction File*, Swarthmore: Joint Committee on Powder Diffraction Standards.

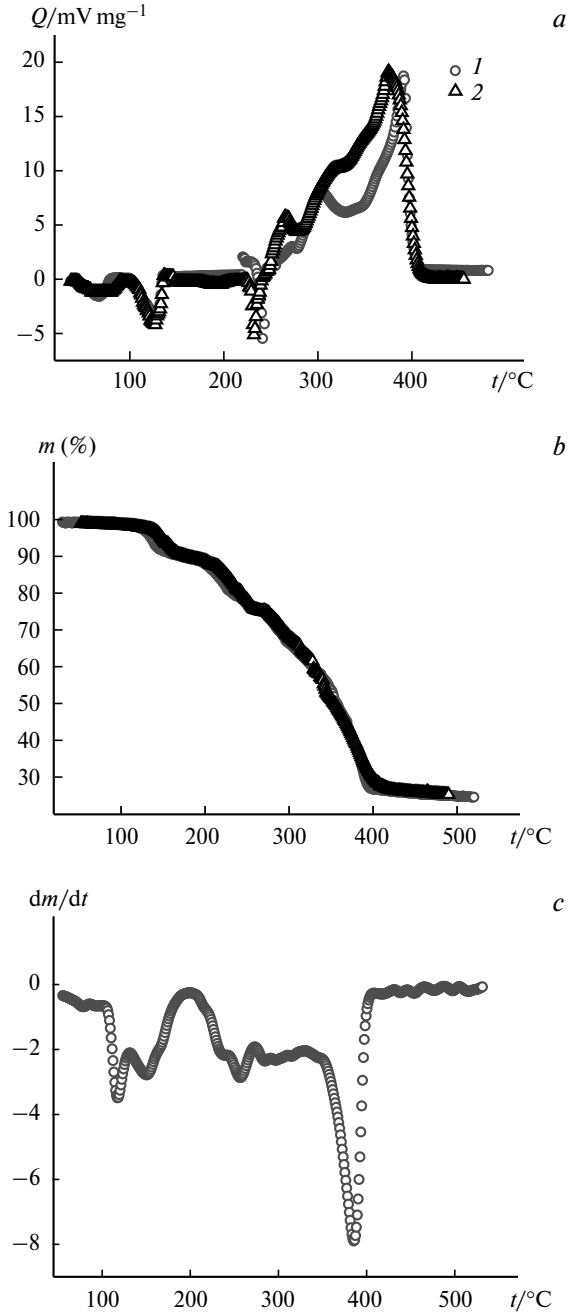

Fig. 9. Temperature dependences of the heat flux (*a*) and the weight loss (*b*) on heating complexes **6** (*1*) and **7** (*2*) and the DTG curve for **6** (*c*) in air (*m*(%), *t*/°C) according to the DSC data.

3 program,[26] which can be employed to perform both the non-*a-priori*[27—29] and model-dependent analysis.[30]

In some cases, the non-*a-priori* analysis of thermoanalytical (TMA) data provides a reliable estimate of the number of reaction steps and the parameters of kinetic equations. Certain knowledge of the mechanism of complex reactions can be gained and the E_A values of their elementary steps can be estimated from the shape of the calculated plots of the activation energy E_A *versus* the conversion x.[31—35] The model-dependent analysis of TMA data cannot be considered as a tool for the elucidation of the true reaction mechanism, but it allows one to efficiently use limited experimental data for the solution of practical problems. This analysis results in the development of the formal model of the process providing the basis for the optimization of the conditions using computational methods in accordance with the problem at hand or for the prediction of the results under specified conditions.[25,31,32]

The analysis was based on the non-isothermal TGA curves obtained during heating of samples at three constant rates (10, 20, and 40 deg min^{-1}). The calculated models were discriminated on the basis of the correlation coefficients r and rms deviations. The correctness of the model was assessed with the Fisher criterion. As can be seen from Fig. 9, *c*, the differential thermogravimetric (DTG) curve has seven well-resolved peaks, and each peak can correspond to either one elementary step or be a result of the superposition of two or several processes.

The non-*a-priori* analysis of multi-step experimental curves were used to construct the plot of the activation energy E_A, which serves as the criterion for the presence of several steps, *versus* the conversion (Fig. 10). The coordinates of special points in Fig. 10 (Table 5) provide an estimate of the lower (maximum points) and upper (minimum points) limits of the activation energies of individual steps. The activation energy in the range $x = 0$—0.05 (the first peak in the DTG) sharply decreases (Fig. 10), and the curve has a concave shape, which is characteristic of processes with the first reversible step (for example, the dehydration of crystal hydrates).[36] In this case, the E_A value calculated from isoconversion lines (see Table 5) for the lowest conversion is equal to the sum of the enthalpy of the reversible step ΔH_r and the activation energy of the following irreversible reaction. Then $\Delta H_r \approx 110 - 50 = 60$ kJ mol^{-1}, which is not contradictory to the enthalpy

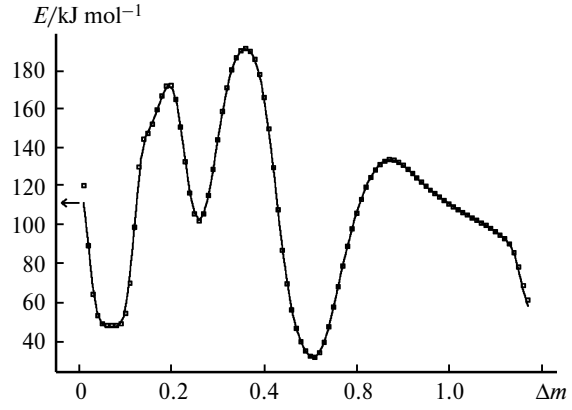

Fig. 10. Plot of the activation energy *versus* the degree of thermolysis of **6** (Friedman method[25]), Δm is the weight loss.

Table 5. Coordinates of special points in the $E_A(x)$ curve (Friedman method[25])

t/°C	*x*	E_A/kJ mol^{-1}
100—200	0.005	110
—	0.070	50
—	0.150	150
200—250	0.200	170
250—280	0.260	100
—	0.360	190
280—380	0.510	32
380—500	0.670	133
—	0.940	85

of sublimation of HPiv (73.2 kJ mol^{-1}). Then the ascending branch of the $E(x)$ curve has an inflection point at $x = 0.15$, which may be attributed to the superposition of subsequent reaction steps. In the third step, $E(x)$ increases from 100 to 190 kJ mol^{-1}. In this case, the optimized coefficient E_A is the effective parameter. For successive reactions, this value can be estimated by the summation of the activation energies of elementary stepts. This region of the $E(x)$ curve in the Friedman plot can be interpreted as the superposition of two elementary reaction steps with the activation energies of about 100 and 190 kJ mol^{-1} and $E_A^{eff} = E_{A,1} + E_{A,2} \approx 100 + 190 = 290$ kJ mol^{-1}. An analysis of the shape of the DTG curve (see Fig. 9, *c*) and the ratio of the slopes of the isoconversion lines and experimental curves in the Friedman plot (Fig. 11) indicate that the final step of the thermolysis occurs with self-acceleration. This hypothesis is quite reasonable, because the thermal decomposition of solid compounds, in particular, of oxalates of some metals is accompanied by the surface fracturing and this, apparently, causes autocatalytic transformations.[37]

Therefore, the non-*a-priori* analysis revealed five formal steps of the process (some of them are not elementary), which provided the basis for the analysis involving the construction of models. By varying the type of kinetic equations in each step,[25] we obtained a series of mathematical models of the process. The statistical criteria and the agreement between the results and the data of the isoconversion analysis allowed us to choose one model as the most probable one. This model (Table 6) includes five sequential steps, the first four steps being described by the *n*-order equations (F_n) (1) and the last step being autocatalytic (C_n) (2):

$$f(x) = F_n + (1 - x)^n, \quad (1)$$

where $f(x)$ is the function determining the dependence of the reaction rate on the conversion, and n is the coefficient to be optimized,

$$f(x) = C_n = (1 - x)^n(1 + K_{cat}X), \quad (2)$$

where K_{cat} and n are the parameters of the regression equations that are optimized.

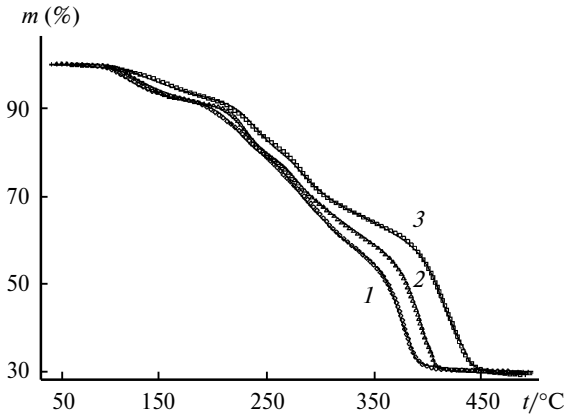

Fig. 11. Experimental TGA curves for the decomposition of complex **6**: the heating rate is 40 deg min^{-1} (*1*), 20 deg min^{-1} (*2*), and 10 deg min^{-1} (*3*).

Table 6. Formal activation energies for the steps in the scheme of thermolysis of **6** (model-dependent analysis)

Steps	*t*/°C	E_A/kJ mol^{-1}
1	100—200	75
2	200—250	150
3	250—280	310
4	280—380	28
5	380—500	140

The thermal decomposition of complex **6** is a complex multi-step process. In the first step, coordinated HPiv molecules are reversibly eliminated. The rate of the backward reaction sharply decreases with an increase in the temperature. The next step involves at least five successive steps, the latter being autocatalytic. Despite the complex mechanism of the thermolysis of the complex, we successfully used the TGA data for the construction of the formal mathematical model of the process suitable for the optimization of the conditions for the preparation of the target product. The correctness of the model is confirmed by the statistical criteria and the agreement between the results and the data obtained by isoconversion methods.

Therefore, the thermal analysis showed that, when heated at relatively low temperatures, the supramolecular structure of binuclear complexes of 3*d*- and 4*f*-block elements with pivalate anions having a similar metal core is broken down (for **2**—**5**) regardless of the atmosphere used for the reaction. The thermal stability is determined by the nature of coordinated neutral ligands (Table 7). The stability of the cobalt-containing complexes is higher than that of the nickel-containing complexes with the similar ligand composition, whereas gadolinium-containing com-

Table 7. Characteristics of the thermal decomposition of compounds **2**—**7** in air

Compound	T_o[a]	T_{ox}[b]	T_f[c]
	°C		
2	105	270	420
3	96[d]	300	475
4	113	280	423
5	102[d]	310	485
6	120	280	397
7	140	285	420

[a] The decomposition onset temperature for the complex.
[b] The temperature for the onset of the oxidative destruction of the metal core.
[c] The temperature for the completion of the decomposition.
[d] Without taking into account the solvent molecules.

plexes are thermally more stable in the corresponding pairs. The thermolysis of the cobalt-containing complexes in an inert atmosphere affords a volatile cobalt-containing intermediate, and the solid decomposition product contains rare earth oxides. The thermolysis of these complexes in air proceeds as the oxidative destruction and should lead to the formation of the corresponding cobaltates in the solid products, which was observed also for complex **2**. The decomposition of the nickel-containing complexes occurs through a somewhat different mechanism. Both in an inert atmosphere and in air, the process produces an intermediate containing an N-donor ligand, whose decomposition in an inert atmosphere is accompanied by the intramolecular redox reaction. For the copper-containing complexes, the steps of elimination of low- and high-boiling-point ligands are rather clear-cut. It shows that the temperature of the destruction of the metal core for complexes of the same rare earth metal is determined by the nature of the 3d metal.

It can be supposed that the decomposition in air should afford rare earth cobaltates and nickelates as the solid products, because the ratio of the metals in the complexes is 1 : 1. It is known that the compound of the composition $LnCoO_3$ is the stable complex oxide that is present in Ln—Co—O systems (Ln = Sm, Eu, Gd).[38] This compound is synthesized by the solid-state method in air by the long-term annealing (≈300 h) of oxide mixtures in the temperature range of 800—1100 °C. In complex oxides with lanthanides, nickel tends to have lower oxidation states compared to cobalt. Lanthanum cobalt trioxide is relatively easily synthesized, whereas lanthanum nickelate $LaNiO_3$ can be prepared only in the flux either under an oxygen flow or under an oxygen pressure higher than the atmospheric pressure.[39] Other nickelates can be synthesized only under drastic oxidative conditions. In complex oxides, oxidation state +2 is most typical of nickel, and the composition of the complex oxide is Ln_2NiO_4. For complex copper and lanthanide oxides, the tendency to a decrease in the oxidation state of the 3d metal is even more pronounced compared to nickel, and it is enhanced in the series of cobaltates, nickelates, and cuprates. Under oxygen-deficient conditions, it is relatively easy to perform the synthesis of $LnCuO_2$. It was shown that the solid-state thermolysis of the complexes under consideration in air results in the formation of samarium and gadolinium cobaltates ($LnCoO_3$) and cuprates (Ln_2CuO_4) as the solid products. For the nickel-containing complexes, the products obtained by the thermolysis in air contain rare earth oxides and NiO. The results of the present study are consistent with a knowledge of the stability of rare earth cobaltates, nickelates, and cuprates. The formal mathematical model of the thermolysis was constructed. This model is suitable for the optimization of the conditions for the preparation of the target product.

Experimental

New complexes were synthesized with the use of commercial MeCN without additional purification. The starting compounds $(\eta^2\text{-bpy})_2M_2(Piv)_4(H_2O)$ (M = Co, Ni), $Cu_2(Piv)_4(HPiv)_2$, and $Ln_2(Piv)_6(HPiv)_6 \cdot HPiv$ (Ln = Sm, Gd) were synthesized according to known procedures.[14,40—42] Commercial 2,2′-bipyridine (99%, Alfa Aesar) was used. The IR spectra of the complexes were recorded on a Spectrum 65LS Fourier-transform infrared spectrometer (Perkin Elmer) in KBr pellets. The microanalysis was carried out on a Carlo Erba analyzer.

(η^1-Aqua)(η^2-2,2′-bipyridyl-*N*,*N*′)tris(μ_2-trimethylacetato-*O*,*O*′)bis(η^2-trimethylacetato-*O*,*O*′)cobalt(II)samarium(III), (η^2-bpy)CoSm(Piv)$_5$(H_2O) (2). The compounds $(\eta^2\text{-bpy})_2Co_2(Piv)_4(H_2O)$ (0.23 g, 0.27 mmol) and $Sm_2(Piv)_6(HPiv)_6 \cdot HPiv$ (0.40 g, 0.27 mmol) in MeCN (20 mL) were stirred with heating (80 °C) for 30 min until the reagents were completely dissolved. The pink solution was concentrated at 60 °C to 10 mL and kept at room temperature for 24 h. The pink crystals suitable for X-ray diffraction were separated from the solution by decantation, washed with cold MeCN, and dried in air. The yield of compound **2** was 0.39 g (80%). Found (%): C, 47.2; H, 6.1; N, 3.1. $C_{35}H_{55}CoN_2O_{11}Sm$. Calculated (%): C, 47.28; H, 6.23; N, 3.15. IR, ν/cm^{-1}: 3419 w, 3110 v.w, 3062 v.w, 2960 s, 2927 m, 2869 w, 1606 s, 1567 s, 1484 s, 1459 m, 1442 m, 1422 s, 1377 m, 1362 m, 1319 m, 1227 s, 1173 v.w, 1156 w, 1101 v.w, 1024 w, 937 v.w, 896 w, 806 w, 790 w, 771 m, 738 w, 652 v.w, 632 v.w, 608 w, 562 w, 418 w.

(η^1-Aqua)(η^2-2,2′-bipyridyl-*N*,*N*′)bis(μ_2-trimethylacetato-*O*,*O*′)(μ_2,η^2-trimethylacetato-*O*,*O*′,*O*′)bis(η^2-trimethylacetato-*O*,*O*′)nickel(II)samarium(III), solvate with trimethylacetic acid, (η^2-bpy)NiSm(Piv)$_5$(H_2O)·2HPiv (3·2HPiv). The compounds $(\eta^2\text{-bpy})_2Ni_2(Piv)_4(H_2O)$ (0.51 g, 0.60 mmol) and $Sm_2(Piv)_6(HPiv)_6 \cdot HPiv$ (0.97 g, 0.60 mmol) in MeCN (20 mL) were stirred with heating (80 °C) for 30 min until the reagents were completely dissolved. The resulting green solution was concentrated at 60 °C to 10 mL and kept at room temperature for 24 h. The green crystals suitable for X-ray diffraction were separated from the solution by decantation, washed with cold MeCN, and dried in air. The yield of compound **3** was 1.04 g (~80%). Found (%): C, 49.6; H, 6.6; N, 2.4. $C_{45}H_{73}N_2NiO_{15}Sm$. Calcu-

lated (%): C, 49.54; H, 6.74; N, 2.57. IR, ν/cm^{-1}: 3352 w, 3275 w, 3108 w, 3064 w, 3036 w, 2972 s, 2933 m, 2874 w, 1599 s, 1550 m, 1532 m, 1484 s, 1460 m, 1447 m, 1361 m, 1378 m, 1320 w, 1226 m, 1189 m, 1103 v.w, 1057 w, 1029 w, 902 m, 867 w, 809 w, 792 w, 773 w, 738 w, 656 v.w, 609 w, 570 w, 419 w.

(η^1-Aqua)(η^2-2,2′-bipyridyl-*N*,*N*′)tris(μ_2-trimethylacetato-*O*,*O*′)bis(η^2-trimethylacetato-*O*,*O*′)cobalt(II)gadolinium(III), (η^2-bpy)CoGd(Piv)$_5$(H_2O) (4). Compound **4** was synthesized analogously to complex **2** with the use of $Gd_2(Piv)_6(HPiv)_6 \cdot HPiv$. The yield was 80%. Found (%): C, 47.1; H, 6.0; N, 2.9. $C_{35}H_{55}CoGdN_2O_{11}$. Calculated (%): C, 46.92; H, 6.19; N, 3.13. IR, ν/cm^{-1}: 3422 w, 3108 v.w, 3062 v.w, 2960 s, 2927 m, 2868 w, 1606 s, 1566 s, 1484 s, 1458 m, 1443 m, 1423 s, 1376 m, 1361 m, 1320 m, 1228 s, 1173 v.w, 1156 w, 1102 v.w, 1024 w, 936 v.w, 896 w, 808 w, 792 w, 770 m, 740 w, 652 v.w, 632 v.w, 608 w, 562 w, 420 w.

(η^1-Aqua)(η^2-2,2′-bipyridyl-*N*,*N*′)bis(μ_2-trimethylacetato-*O*,*O*′)(μ_2,η^2-trimethylacetato-*O*,*O*′,*O*′)bis(μ^2-trimethylacetato-*O*,*O*′)nickel(II)gadolinium(III), solvate with trimethylacetic acid, (η^2-bpy)NiGd(Piv)$_5$(H_2O)·2HPiv (5·2HPiv). Compound **5** was synthesized analogously to complex **3** with the use of $Gd_2(Piv)_6(HPiv)_6 \cdot HPiv$. The yield was 82%. Found (%): C, 49.3; H, 6.6; N, 2.6. $C_{45}H_{73}GdN_2NiO_{15}$. Calculated (%): C, 49.22; H, 6.70; N, 2.55. IR, ν/cm^{-1}: 3352 w, 3278 w, 3107 w, 3064 w, 3035 w, 2970 s, 2931 m, 2875 w, 1601 s, 1552 m, 1532 m, 1484 s, 1461 m, 1447 m, 1361 m, 1380 m, 1321 w, 1226 m, 1190 m, 1102 v.w, 1056 w, 1030 w, 902 m, 867 w, 807 w, 792 w, 774 w, 738 w, 656 v.w, 609 w, 570 w, 420 w.

(η^2-2,2′-Bipyridyl-*N*,*N*′)(η^1-trimethylacetic acid-*O*)bis(μ_2-trimethylacetato-*O*,*O*′)(μ_2,η^2-trimethylacetato-*O*,*O*′,*O*′) (η^1-trimethylacetato-*O*,*O*′)(η^2-trimethylacetato-*O*,*O*′)copper(II)samarium(III), (η^2-bpy)CuSm(Piv)$_5$(HPiv) (6). 2,2′-Bipyridine (0.09 g, 0.6 mmol) was added to a solution of $Cu_2(Piv)_4(HPiv)_2$ (0.2 g, 0.3 mmol) in MeCN (40 mL), and the reaction mixture was stirred with heating (80 °C) for 30 min. Then $Sm_2(Piv)_6(HPiv)_6 \cdot HPiv$ (0.49 g, 0.3 mmol) was added to the resulting green-blue solution, and the mixture was stirred with heating (80 °C) for 1 h. The resulting green solution was filtered off, concentrated to 20 mL, and kept at room temperature for 24 h. The dark-green crystals suitable for X-ray diffraction were separated from the solution by decantation, washed with cold MeCN, and dried in air. The yield of compound **6** was 0.44 g (~75%). Found (%): C, 49.0; H, 6.4; N, 2.7. $C_{40}H_{63}CuN_2O_{12}Sm$. Calculated (%): C, 49.13; H, 6.49; N, 2.86. IR (KBr), ν/cm^{-1}: 3436 w, 3105 v.w, 3082 v.w, 3058 v.w, 2973 w, 2929 m, 2869 w, 1585 s, 1574 s, 1552 s, 1516 s, 1484 s, 1447 m, 1427 s, 1378 m, 1361 m, 1317 w, 1281 v.w, 1277 m, 1178 v.w, 1160 v.w, 1106 v.w, 1058 v.w, 1031 w, 1016 w, 989 v.w, 937 v.w, 894 m, 795 w, 779 m, 734 w, 660 w, 604 m, 576 w, 420 w.

(η^2-2,2′-Bipyridyl-*N*,*N*′)(η^1-trimethylacetic acid-*O*)bis(μ_2-trimethylacetato-*O*,*O*′)(μ_2,η^2-trimethylacetato-*O*,*O*′,O′) (η^1-trimethylacetato-*O*,*O*′)(η^2-trimethylacetato-*O*,*O*′)copper(II)-gadolinium(III), (η^2-bpy)CuGd(Piv)$_5$(HPiv) (7). Compound **7** was synthesized analogously to complex **6** with the use of $Gd_2(Piv)_6(HPiv)_6 \cdot HPiv$. The yield was 72%. Found (%): C, 48.6; H, 6.5; N, 2.7. $C_{40}H_{63}CuGdN_2O_{12}$. Calculated (%): C, 48.79; H, 6.45; N, 2.84. IR (KBr), ν/cm^{-1}: 3435 w, 3104 v.w, 3081 v.w, 3058 v.w, 2970 w, 2930 m, 2866 w, 1585 s, 1573 s, 1552 s, 1516 s, 1483 s, 1446 m, 1427 s, 1378 m, 1360 m, 1317 w, 1280 v.w, 1277 m, 1177 v.w, 1159 v.w, 1106 v.w, 1059 v.w, 1031 w, 1016 w,

Table 8. Crystallographic parameters for **2**, **3**, and **7**

Compound	**2**	**3**	**7**
Molecular formula	$C_{35}H_{55}CoN_2O_{11}Sm$	$C_{45}H_{73}N_2NiO_{15}Sm$	$C_{40}H_{63}CuGdN_2O_{12}$
M/g mol^{-1}	889.09	1093.13	984.71
T/K	293(2)	293(2)	296(2)
Crystal system	Monoclinic	Triclinic	Monoclinic
Space group	$P2_1/n$	$P\bar{1}$	$P2_1/c$
a/Å	14.538(5)	12.1686(18)	22.722(2)
b/Å	17.018(6)	15.114(2)	11.3837(12)
c/Å	17.241(6)	16.203(2)	20.936(2)
α/deg	90	88.005(2)	90
β/deg	90.014(1)	69.169(2)	113.937(2)
γ/deg	90	88.296(2)	90
V/Å^3	4266(3)	2783.0(7)	4949.5(9)
Z	4	2	4
ρ_{calc}/g cm^{-3}	1.384	1.304	1.321
μ/mm^{-3}	1.805	1.442	1.811
θ_{max}/deg	24.63	28.28	26.42
T_{min}/T_{max}	—	0.6716/0.9857	0.6126/0.9149
Number of measured reflections	31983	29246	28803
Number of reflections with $I > 2\sigma(I)$	4629	11881	6104
R_{int}	0.1453	0.0571	0.0607
GOOF	1.043	1.047	1.038
R_1 ($I > 2\sigma(I)$)	0.0498	0.0334	0.0658
wR_2 ($I > 2\sigma(I)$)	0.1070	0.0844	0.1562

989 v.w, 937 v.w, 895 m, 794 w, 779 m, 734 w, 660 w, 605 m, 577 w, 421 w.

The X-ray diffraction data for complexes **2**, **3**·HPiv, and **7** were collected on a Bruker Apex II diffractometer equipped with a CCD detector (MoKα, λ = 0.71073 Å, graphite monochromator) using the standard technique.[43] For compounds **3**·2HPiv and **7**, a semiempirical absorption correction was applied.[44] The structures of all complexes were solved by direct methods and refined by the full-matrix least-squares method with anisotropic displacement parameters for all nonhydrogen atoms. The hydrogen atoms of the *tert*-butyl substituents of the pivalate ligands were positioned geometrically and refined using a riding model. All calculations were carried out with the use of the SHELXS-97 and SHELXL-97 program packages.[45] The crystallographic parameters and the structure refinement statistics are given in Table 8.

The thermal decomposition of compounds **2**, **3**, and **6** was studied by differential scanning calorimetry and thermogravimetric analysis on DSC-20 and TG-50 units of a Mettler TA-3000 thermoanalyzer at a heating rate of 10 deg min^{-1}. The weight loss upon thermal decomposition was determined directly on the TG-50 unit; the accuracy of weighing was $\pm 2 \cdot 10^{-3}$ mg. The calibration coefficient for the DSC-20 unit was calculated with the TC-11 automatic processor using the "calibration 1" procedure based on the heat of fusion of a certified indium sample. The calibration correction for a change in the sensitivity of a thermocouple battery was automatically applied depending on the temperature by performing the "calibration 2" procedure. The accuracy of the determination of the temperature and thermal effects in the thermograms was ±1° and ±2.0%, respectively. The weights of the samples were 5—10 mg.

The thermal decomposition of complexes **4**, **5**, and **7** was studied by differential scanning calorimetry (DSC) and thermogravimetric analysis (TGA) on NETZSCH instruments. The thermogravimetric measurements were carried out in a flow of artificial air (O_2, 20.8%; CH_4, < 0.0001%) (20 mL min^{-1}) and argon (Ar, > 99.998%; O_2, < 0.0002%; N_2, < 0.001%; water vapor, < 0.0003%; CH_4, < 0.0001%) (20 mL min^{-1}) on a TG 209 F1 instrument in alundum crucibles at a heating rate of 10 deg min^{-1}. The composition of the gas phase was studied on a QMS 403C Aeolos mass-spectrometric unit under TGA conditions. The ionizing electron energy was 70 eV; the maximum determined mass number (the ratio of the mass of the ion to its charge Z) was 300 amu. The weights of the samples used in thermogravimetric experiments were 0.5—3 mg. Studies by differential scanning calorimetry under a dry artificial air and argon flow were carried out on a DSC 204 F1 calorimeter in aluminum cells at a heating rate of 10 deg min^{-1}. The weights of the samples were 4—10 mg. The temperature calibration of the thermobalance and the calorimeter was performed based on the phase transition points of the reference compounds (C_6H_{12}, Hg, KNO_3, In, Sn, Bi, CsCl, 99.99% purity) according to the ISO/CD 11357-1 standard. The samples used for the TGA and DSC experiments were weighed on a SARTORIUS RESEARCH R 160P analytical balance with an accuracy of $1 \cdot 10^{-2}$ mg.

The X-ray powder diffraction analysis of the thermolysis products was carried out with a FR-552 monochromator chamber ($CuK\alpha_1$ radiation) using germanium as the internal standard (X-ray diffraction patterns were processed with an IZA-2 comparator with an accuracy of ±0.01 mm) and a STOE Powder Diffraction System.

The study was performed in part using scientific equipment of the Joint Use Center of the M. V. Lomonosov Moscow State University.

This study was financially supported by the Russian Foundation for Basic Research (Project No 11-03-12150), the Council on Grants of the President of the Russian Federation (Program for State Support of Leading Scientific Schools and Young Scientists of the Russian Federation, Grants MK-1185.2011.3, NSh-2357.2012.3, and NSh-1670.2012.3), the Ministry of Education and Science of the Russian Federation (Federal Contracts P850 and 14.740.11.0363), the Division of Chemistry and Materials Science of the Russian Academy of Sciences, and the Presidium of the Russian Academy of Sciences.

References

1. M. Sakamoto, K. Manseki, H. Okawa, *Coord. Chem. Rev.*, 2001, **219**, 379.
2. H. H. Wang, K. D. Carlson, U. Geiser, R. J. Thorn, H.-C. I. Kao, M. A.Beno, M. R. Monnghan, T. J. Allen, R. B. Proksch, D. L. Stupka, J. M. Williams, B. K. Flandermeyer, R. B. Poeppel, *Inorg. Chem.*, 1987, **26**, 1476.
3. S. Wang, Z. Pang, K. D. L. Smith, M. J. Wagner, *J. Chem. Soc., Dalton Trans.*, 1994, 955.
4. L. Chen, S. R. Breeze, R. J. Rousseau, J. S. Wang, L. K. Thompson, *Inorg. Chem.*, 1995, **34**, 454.
5. R. A. Reynolds, D. Coucouvanis, *J. Am. Chem. Soc.*, 1998, **120**, 209.
6. O. Carp, L. Patron, A. Ianculescu, D. Crisan, N. Lragan, R. Olar, *J. Therm. Anal. Calorim.*, 2003, **72**, 253.
7. A. V. Kharchenko, A. M. Makarevich, A. N. Grigoriev, N. M. Sorokina, K. A. Lyssenko, N. P. Kuzmina, *Dokl. Akad. Nauk*, 2009, **426**, 497 [*Dokl. Chem.* (*Engl. Transl.*), 2009, **426**, 124].
8. L. Patron, O. Carp, I. Madru, G. Grasa, *J. Therm. Anal. Calorim.*, 1999, **56**, 597.
9. Y. Sadaoka, K. Watanabe, Y. Sakai, M. Sakamoto, *J. Alloys Comp.*, 1995, **222**, 194.
10. M. A. Bykov, A. L. Emelina, M. A. Kiskin, G. G. Aleksandrov, A. S. Bogomyakov, Zh. V. Dobrokhotova, V. M. Novotortsev, I. L. Eremenko, *Zh. Neorg. Khim.,* 2009, **54**. 601 [*Russ. J. Inorg. Chem.* (*Engl. Transl.*), 2009, **54**, 548].
11. N. Deb, *J. Therm. Anal. Calorim.*, 2002, **67**, 699.
12. O. Carp, L. Patron, A. Ianculescu, D. Crisan, N. Lragan, R. Olar, *J. Therm. Anal. Calorim.*, 2003, **72**, 253.
13. I. L. Eremenko, S. E. Nefedov, A. A. Sidorov, I. I. Moiseev, *Izv. Akad. Nauk, Ser. Khim.*, 1999, 409 [*Russ. Chem. Bull.* (*Engl. Transl.*), 1999, **48**, 405].
14. I. L. Eremenko, S. E. Nefedov, A. A. Sidorov, M. A. Golubnichaya, P. V. Danilov, V. N. Ikorskii, Yu. G. Shvedenkov, V. M. Novotortsev, I. I. Moiseev, *Inorg. Chem.*, 1999, **38**, 3764.
15. I. L. Eremenko, A. A. Sidorov, G. G. Aleksandrov, *Ros. Khim. Zh.*, 2004, **48**, 126 [*Mendeleev Chem. J.* (*Engl. Transl.*), 2004, **48**].
16. J.-H. Liao, C.-T. Su, C.-C. Hsu, *Acta Crystallogr.*, *Sect. E: Struct. Rep. Online*, 2001, **57**, m 501.

17. M. Kurmoo, C. Estournes, Y. Oka, H. Kumagai, K. Inoue, *Inorg. Chem.*, 2005, **44**, 217.
18. I. S. Evstifeev, M. A. Kiskin, V. S. Mironov, A. S. Bogomyakov, A. A. Sidorov, V. M. Novotortsev, I. L. Eremenko, *Inorg. Chem. Comm.*, 2010, **13**, 498.
19. I. Fomina, Z. Dobrokhotova, G. Aleksandrova, A. Bogomyakov, M. Fedin, A. Dolganov, T. Magdesieva, V. Novotortsev, I. Eremenko, *Polyhedron*, 2010, **29**, 1734.
20. A. W. Addison, T. N. Rao, *J. Chem. Soc., Dalton Trans.*, 1984, 1349.
21. A. Albinati, V. I. Bakhmutov, N. V. Belkova, C. Bianchini, L. Epstein, I. de los Ríos, E. I. Gutsul, L. Marvelli, M. Peruzzini, R. Rossi, E. Shubina, E. V. Vorontsov, F. Zanobini, *Eur. J. Inorg. Chem.*, 2002, 1530.
22. Zh. V. Dobrokhotova, I. G. Fomina, M. A. Kiskin, A. A. Sidorov, V. M. Novotortsev, I. L. Eremenko, *Izv. Akad. Nauk, Ser. Khim.*, 2006, 250 [*Russ. Chem. Bull.*, *Int. Ed.*, 2006, **55**, 256].
23. I. G. Fomina, G. G. Aleksandrov, Zh. V. Dobrokhotova, O. Yu. Proshenkina, M. A. Kiskin, Yu. A. Velikodnyi, V. N. Ikorskii, V. M. Novotortsev, I. L. Eremenko, *Izv. Akad. Nauk*, *Ser. Khim.*, 2006, 1841 [*Russ. Chem. Bull., Int. Ed.*, 2006, **55**, 1909].
24. http://webbook.nist.gov.
25. J. Opfermann, *J. Therm. Anal. Cal.*, 2000, **60**, 641.
26. H. L. Friedman, *J. Polymer Lett.*, 1966, **4**, 323.
27. T. Ozawa, *Bull. Chem. Soc. Jpn*, 1965, **38**, 1881.
28. J. Flynn, L. A. Wall, *J. Polymer Lett.*, 1966, **4**, 232.
29. J. Opfermann, E. Kaisersberger, *Thermochim. Acta*, 1992, **203**, 167.
30. H.-J. Flammersheim, J. R. Opfermann, *Thermochim. Acta*, 2002, **388**, 389.
31. M. E. Brown, M. Maciejewski, S. Vyazovkin, R. Nomen, J. Sempre, A. Burnham, J. Opfermann, R. Strey, H. L. Anderson, A. Kemmler, R. Keuleers, J. Janssens, H. O. Desseyn, Ch.-R. Li, T. B. Tang, B. Roduit, J. Malek, T. Mitsuhashi, *Thermochim. Acta*, 2000, **355**, 125.
32. M. Maciejewski, *Thermochim. Acta*, 2000, **355**, 145.
33. S. Vyazovkin, *Thermochim. Acta*, 2000, **355**, 155.
34. A. Burnham, *Thermochim. Acta*, 2000, **355**, 165.
35. H. J. Flammersheim, *Thermochim. Acta*, 2000, **361**, 21.
36. S. V. Vyazovkin, A. I. Lesnikovich, *Thermochim. Acta*, 1990, **165**, 273.
37. G. M. Zhabrova, B. M. Kadenatsi, O. V. Krylov, A. V. Shkarin, V. A. Gordeeva, *Teor. Eksp. Khim.*, 1970, **6**, No. 2, 198 [*Theor. Exp. Chem.* (*Engl. Transl.*), 1970, **6**].
38. A. Yu. Kropanev, A. N. Petrov, V. M. Zhukovskii, *Zh. Neorg. Khim.,* 1983, **28**, 2938 [*J. Inorg. Chem. USSR* (*Engl. Transl.*), 1983, **28**, No. 11].
39. L. M. Golub, L. S. Sidorik, S. A. Nedil´ko, T. I. Fedoruk, *Izv. Akad. Nauk SSSR, Ser. Neorg. Mater.*, 1978, **14**. 1866 [*Bull. Acad Sci. USSR, Ser. Inorg. Mater.* (*Engl. Transl.*), 1978, **14**].
40. A. A. Sidorov, Dr. Sc. (Chem.) Thesis, N. S. Kurnakov Institute of General and Inorganic Chemistry, Russian Academy of Sciences, Moscow, 2002, pp. 221 (in Russian).
41. T. O. Denisova, E. V. Amel´chenkova, I. V. Pruss, Zh. V. Dobrokhotova, O. F. Fialkovskii, S. E. Nefedov, *Zh. Neorg. Khim.,* 2006, **51**, 1098 [*Russ. J. Inorg. Chem.* (*Engl. Transl.*), 2006, **51**, 1020].
42. I. G. Fomina, M. A. Kiskin, A. G. Martynov, G. G. Aleksandrov, Zh. V. Dobrokhotova, Yu. G. Gorbunova, Yu. G. Shvedenkov, A. Yu. Tsivadze, V. M. Novotortsev, I. L. Eremenko, *Zh. Neorg. Khim.,* 2004, **49**, 1463 [*Russ. J. Inorg. Chem.* (*Engl. Transl.*), 2004, **49**, 1349].
43. *SMART (Control) and SAINT (Integration) Software, Version 5.0*, Bruker AXS Inc., Madison, WI, 1997.
44. G. M. Sheldrik, *SADABS, Program for Scanning and Correction of Area Detector Data*, Götinngen University, Götinngen, Germany, 2004.
45. G. M. Sheldrick, *Acta. Crystallogr.*, 2008, **A64**, 112.

Received May 4 2011;
in revised form October 13, 2011